Bioorg. Med. Chem. Lett. 42 (2021) 128062

Contents lists available at ScienceDirect

Bioorganic & Medicinal Chemistry Letters

journal homepage: www.elsevier.com/locate/bmcl

Discovery of boronic acid-based potent activators of tumor pyruvate kinase M2 and development of gastroretentive nanoformulation for oral dosing

Rajkumar Patle [a,1], Shital Shinde [a], Sagarkumar Patel [a,1], Rahul Maheshwari [b], Heena Jariyal [c], Akshay Srivastava [c], Neelam Chauhan [c], Christoph Globisch [d], Alok Jain [c], Rakesh K. Tekade [b,*], Amit Shard [a,*]

[a] Department of Medicinal Chemistry, National Institute of Pharmaceutical Education and Research-Ahmedabad, India
[b] Department of Pharmaceutics, National Institute of Pharmaceutical Education and Research-Ahmedabad, India
[c] Department of Biotechnology, National Institute of Pharmaceutical Education and Research-Ahmedabad, India
[d] Department of Chemistry, University of Konstanz, Germany

ARTICLE INFO

Keywords:
Cancer
Pyruvate kinase M2
Boronic acid
Nanoformulation
MD simulations
Thiolatedchitosan-based nanoparticles (TCNPs)

ABSTRACT

Several studies have established that cancer cells explicitly over-express the less active isoform of pyruvate kinase M2 (PKM2) is critical for tumorigenesis. The activation of PKM2 towards tetramer formation may increase affinity towards phosphoenolpyruvate (PEP) and avoidance of the Warburg effect. Herein, we describe the design, synthesis, and development of boronic acid-based molecules as activators of PKM2. The designed molecules were inspired by existing anticancer scaffolds and several fragments were assembled in the derivatives. **6a-6d** were synthesized using a multi-step synthetic strategy in 55–70% yields, starting from cheap and readily available materials. The compounds were selectively cytotoxic to kill the cancerous cells at 80 nM, while they were non-toxic to the normal cells. The kinetic studies established the compounds as novel activators of PKM2 and (*E/Z*)-(4-(3-(2-((4-chlorophenyl)amino)-4-(dimethylamino)thiazol-5-yl)-2-(ethoxycarbonyl)-3-oxoprop-1-en-1-yl) phenyl)boronic acid (**6c)** emerged as the most potent derivative. **6c** was further evaluated using various *in silico* tools to understand the molecular mechanism of tetramer formation. Docking studies revealed that **6c** binds to the PKM2 dimer at the dimeric interface. Further to ascertain the binding site and mechanism of action, rigorous MD (molecular dynamics) simulations were undertaken, which led to the conclusion that **6c** stabilizes the center of the dimeric interface that possibly promotes tetramer formation. We further planned to make a tablet of the developed molecule for oral delivery, but it was seriously impeded owing to poor aqueous solubility of **6c**. To improve aqueous solubility and retain **6c** at the lower gastrointestinal tract, thiolated chitosan-based nanoparticles (TCNPs) were prepared and further developed as tablet dosage form to retain anticancer potency in the excised goat colon. Our findings may provide a valuable pharmacological mechanism for understanding metabolic underpinnings that may aid in the clinical development of new anticancer agents targeting PKM2.

Pyruvate kinase is one of the critical metabolic conduits that catalyzes the bio-energetically enriched terminal step in glycolysis.[1] It converts phosphoenolpyruvate (PEP) to pyruvate and produces ATP for energy production.[2] There are four isoforms of pyruvate kinase (PK) isoenzyme: PKLR (liver isoform L-PK), R-PK (red blood cell isoform), M1-PK (muscle isoform), and PKM2 (Pyruvate kinase M2 present in embryonic and tumor cells) forms.[3] Out of all isoforms, PKM2 is deeply associated with tumor growth, survival, and metastasis.[4] PKM2 active state (tetrameric) has more affinity towards PEP, whereas dimeric PKM2 is inactive and has a very low affinity towards PEP.[5] The tetrameric form drags the glycolysis towards pyruvate synthesis. Fructose 1,6 bisphosphate (FBP) and serine are natural allosteric activators of PKM2, which catalyze the tetramer's formation.[6] However, the dimeric PKM2 in tumor tissues leads to the accumulation of glycolysis intermediates resulting in activation of alternate metabolic pathways.[7]

The present research is focused on developing compounds that

* Corresponding authors.
E-mail addresses: rakeshtekade@niperahm.ac.in (R.K. Tekade), amit@niperahm.ac.in (A. Shard).
[1] Authors contributed equally

https://doi.org/10.1016/j.bmcl.2021.128062
Received 10 January 2021; Received in revised form 17 April 2021; Accepted 21 April 2021
Available online 24 April 2021

activate PKM2 and act as potent anticancer agents.[8] The much-studied compounds are micheolide, Ml-265, DASA-58, SAICAR, and its derivatives.[9–12] Some promising PKM2 activators having appreciable biological potential are shown in Fig. 1. Covalent modifiers like micheliode onsets covalent modification of target leading to anticancer effects. However, its applicability has been largely impeded owing to associated safety concerns.[13] Several studies have demonstrated significant synergistic effects of PKM2 modulators in combination with other wide range of established oncology drugs.[14] It is imperative to mention that the development of kinase activators will be highly useful as it will smartly bypass the functional consequences associated with kinase inhibitors.[15] On the contrary, activator binding may stabilize the binding-competent state. This may increase the target affinity and often pushes the dynamic range to lower target concentrations.[16]

Thus, there is a need to develop novel PKM2 activators as anticancer agents. It has been demonstrated that boronic acid-based molecules are electrophilic and potent antiproliferative agents.[17–21] For instance, bortezomib is chiefly employed in multiple myelocytic leukemia, and targets the serine/threonine amino acids of proteasome through its electrophilic boronic acid core (Fig. 2).[22] Boron-containing functional groups like diazaborines, boronic acids, esters, and benzoxaboroles have been successfully incorporated into therapeutics. Aryl boronic acids also provide a viable biomimetic of phenolic group having poor bioavailability profiles.[23]

Boronic acid functional group improves the water solubility of potent anticancer combretastatin CA-4. The moiety also increases the lipophilicity and affinity of a drug towards the hydrophobic region of the receptor. It can improve the stability of a drug towards metabolic degradation.[24] At the cell surface, an intense cluster of polysaccharides is present that forms glycocalyx. The boronic acids can readily form boronate esters with glycocalyx that may enhance drug selectivity towards tumor cells.[25] The widespread utility of boronic acids stems from its vacant p-orbital of boron. Boron has chameleonic behavior that switches between electrophilic and nucleophilic states under physiological conditions.[26]

Here, we designed and synthesized four novel compounds based on boronic acids centered around the thiazole core, which is generally considered as master keys in medicinal chemistry.[27–30] We further describe the enzyme assay of the molecules synthesized, their inhibitory effects on various cancer cell lines, including triple-negative breast cancer and mesenchymal stem cells, along with computational studies to elucidate the mechanism of action of our molecules. This was followed by the development of a formulation to target colon cancer reported to have the highest expression of PKM2. Considering the poor aqueous solubility of **6c,** a contemporary nanoparticle-based formulation was developed. Recently *in vitro* metabolite profiling of **6c** was successfully done and published.[31] We speculated that thiolated chitosan-based formulation may enhance mucoadhesion to colon cells and can have a marked impact on gastric retention. Our results strongly support that rationally designed boronic acid-based PKM2 activators can orchestrate multifaceted cancer cell elimination responses. Thus, targeting PKM2 with activators may represent a novel anticancer strategy. Modelling studies suggested that boronic acid scaffold could position itself within proximity of PKM2 dimers which could enhance the binding kinetics.

The idea to synthesize boronic acid-based molecules stemmed from our recent findings where nitrile substituted phenylaminothiazoles (PAT) were found to act as B-cell lymphoma-2 (Bcl-2) inhibitors.[32] The molecules were found to pan assay interference compounds (PAINS) free and had adequate ADMET properties to guide the apoptosis in cancerous cells. Considering PAT moiety (blue highlighted) insignia of anticancer activity, we started tinkering with nitrile moiety isosteric to carbonyl moiety (yellow highlighted) (Fig. 3).

Since we were inclined to target PKM2, we found that 1,3 dicarbonyl moiety (yellow highlighted) existing in curcumin directly modulates PKM2.[33] Upon analyzing the structure, it was further found that Knoevenagel condensation of carbonyl substituted phenylboronic acid with active methylene of 1,3 dicarbonyl moiety yields cinnamate, which is also a known PKM2 modulator.[34] We chose ethyl ester owing to the toxicity of methyl esters. Further, as explained in the introduction, the boronic acid moiety involved in the modulation of kinases was incorporated. Moreover, it may be metabolized to a phenolic moiety (**6c-OH**) by simultaneous generation of non-toxic boric acid.[26]

Further, to synthesize the molecules, phenyl isothiocyanates (**2**) were prepared from aniline (**1**) derivatives and carbon disulfide via dithiocarbamate salt intermediate (Scheme 1).[35] Tetramethylguanidine adducts (**3**) were synthesized by the treatment of isothiocyanate derivatives (**2**) (1 eq.) with 1,1,3,3 tetramethylguanidine (1 eq.) at room temperature.[36]

Tetramethylguanidine adducts (**3**) underwent cyclization in the presence of 4-chloroacetoacetate that led to thiazole-based (**4**) core structure having a side-chain of 1,3 dicarbonyl moiety.[37] Desired compounds (**6a-6d**) were synthesized via the Knoevenagel condensation method (Fig. 4).[38] (For detailed procedure of synthesis, please refer to the supplementary information).

PKM2 dimeric form is a hallmark of cancer, while the tetrameric (active) form is incharge of pyruvate generation. The PKM2 enzyme activity was ascertained by lactate dehydrogenase **(**LDH)-coupled enzyme assay.[39] The results indicated that **6a-6d** are acting as an activator with AC_{50} of 7.15 μM, 6.11 μM, 5.69 μM, and 8.17 μM, respectively. Fig. 5 is showing % relative activity of PKM2 following treatment with **6a-6d**.

To further ascertain the potential of **6a-6d**, we screened them against different cell lines (Table 1). Here, we used a wide range of cancer cell lines, including drug-resistant MDA-MB and drug-sensitive cell lines like MCF-7, Bcl-2 Jurkat, and Colo-201.[40,41] All the cell lines and normal fibroblast cells were also treated with varying concentrations of **6a-6d** and assayed for the cell viability by MTT (3-[4,5-dimethylthiazol-2-yl]-2,5-diphenyl tetrazolium) assay.[42] It is pertinent to mention that all the cell lines are known to have sufficient PKM2 expression. Cell growth was inhibited in all treated cancer cell lines (IC_{50}, 80 nM − 58.7 μM) in a concentration-dependent manner (Table 1). It may be noted that the PKM2 activation at a particular concentration leads to the formation of tetramer and has reverted the cancerous phenotype leading to cytotoxicity.

The MCF-7 cell line was found to be more sensitive to **6c**, with an IC_{50} of 0.08 μM. The activities showed (IC_{50}) in Table 1 established that **6c** showed promise against almost all cell lines at various concentrations.

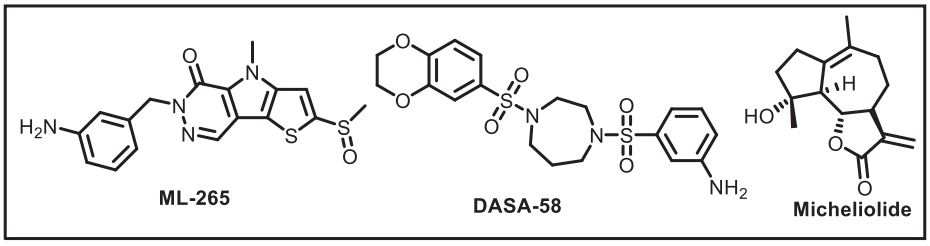

Fig. 1. Reported PKM2 activators (ML-265, DASA-58, Micheliolide).

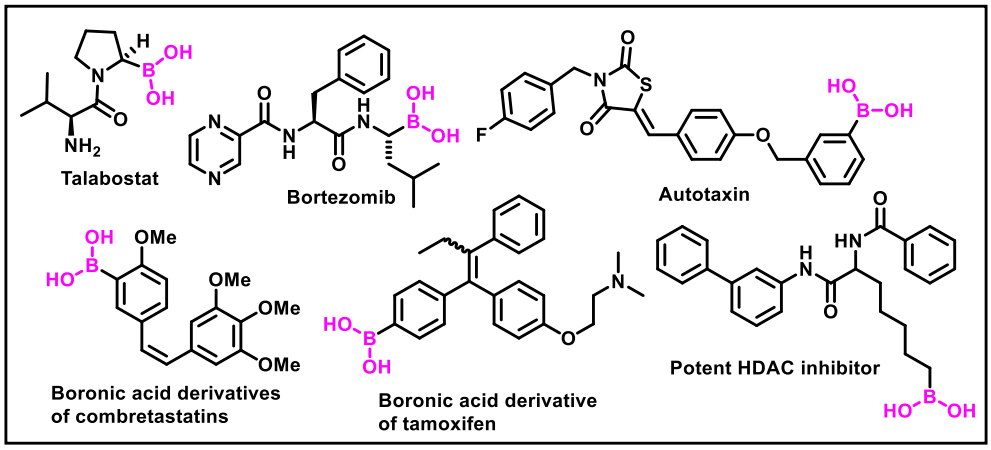

Fig. 2. Boronic acid-based anticancer molecules.

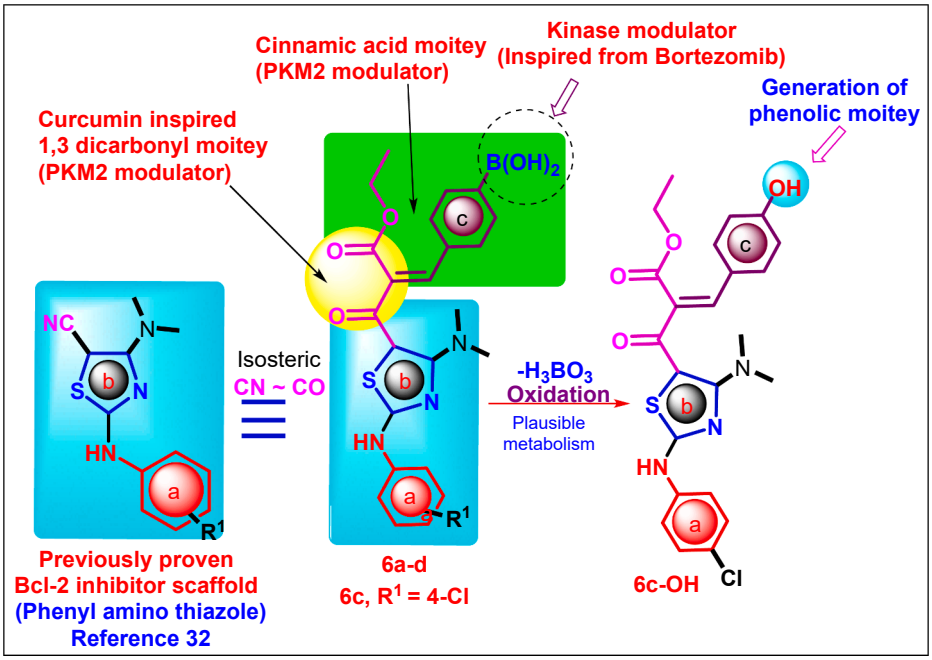

Fig. 3. Design of boronic acid-based moieties and their plausible metabolism.

PKM2 is involved in cellular proliferation, regulation, apoptosis, and metastasis of cancer cells.[43] Annexin PI assay revealed that **6c** induced annexin positive population is 8.81% and double-positive is 23.50% at a much lower concentration of 100 nM of **6c** (Fig. 6).[44] Results indicate that **6c** induces apoptosis at 100 nM. Thus, PKM2 activator (**6c**) induced cytotoxicity at a much lower concentration.

Tetrameric PKM2 is the only form with high pyruvate kinase activity.[45] Cancer cells mainly utilize aerobic glycolysis to meet their proliferative demands.[46] PKM2 occurs in dimeric (inactive) and tetrameric (active) forms inside cells. Cancer cells maintain lower levels of tetrameric form to increase the glucose uptake of cells and utilize them for alternate metabolic pathways.[47] Furthermore, lower levels of the tetrameric form allow the entry of key glycolytic intermediates towards biosynthesis of essential biomolecules, which is required for cell proliferation.[48] Accumulation of glycolytic intermediates in cancer cells can be prevented by converting dimeric PKM2 to tetrameric PKM2. Tetramerization of PKM2 was ascertained by disuccinimidyl suberate (DSS) cross-linker assay.[49] We observed that when MCF-7 cells were treated with **6c,** increased tetramer formation at 250 kDa as compared to control cells (untreated MCF-7 cell) was observed (Fig. 7). Thus, the **6c** compound could be a potent activator of PKM2 and showed antitumor activity *in vitro*.

6c emerged as one of the most bioactive molecules amongst all, and its effect on inhibiting proliferation was subsequently demonstrated in a wide variety of cancer cell lines. It was able to inhibit the growth of different cell lines, as mentioned in Table 1. The compound also showed an increase in percent activity of PKM2 with an AC_{50} of 5.6 μM. Furthermore, **6c** also enhanced the tetramer formation in MCF-7 cells when cells were treated with IC_{50} concentration of compound compared to untreated cells.

The compound **6c** was found to be the most potent analog among the four different boronic acid-based ligands, we tried to evaluate computationally where it binds. The PKM2 monomer consists of 531 amino acids and aggregates in PKM2 into a homotetrameric structure (A, B, C, and D chains). In normal physiological conditions, PKM2 remains in tetramer conformation. However, post-translational modifications or mutations hinder the tetramer formation process, and the equilibrium is shifted towards dimer conformation. Therefore, in the docking study, we only considered the dimeric conformation. Designed molecule **6c** and FBP were docked at the allosteric (FBP binding) site and the interface

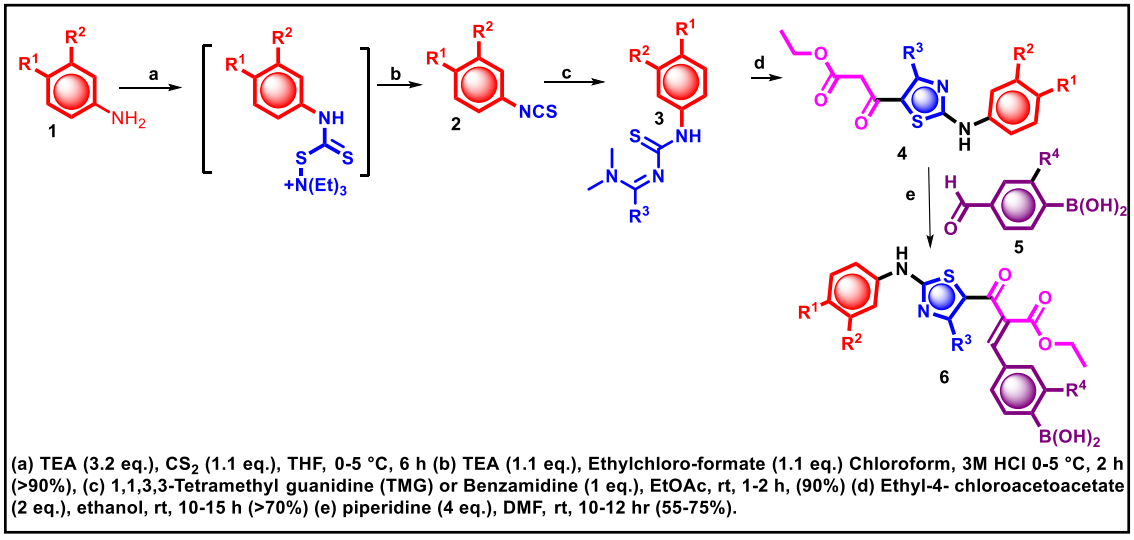

Scheme 1. A generalized scheme for the synthesis of boronic acid-based molecules.

Compound Number	R^1	R^2	R^3	R^4
6a	-H	-H	$-N(CH_3)_2$	-H
6b	-F	-H	$-C_6H_5$	-H
6c	-Cl	-H	$-N(CH_3)_2$	-H
6d	-OMe	-H	$-N(CH_3)_2$	-H

Fig. 4. The desired compounds (6a-6d) and their substitution patterns.

binding site (interface between two chains) as displayed in Fig. 8. Binding energies of **6c** and FBP in dimer conformation at the allosteric site were −51.5 and −97.8 kcal/mol, respectively. The binding energies corroborated very well with non-covalent interaction patterns between ligands and protein. FBP formed a higher number of H-bonds, and participated in salt bridge interaction compared with fewer H-bonds by our designed molecule **6c** at the allosteric sites (Fig. 8).

Similar trends were observed in the binding pattern of FBP at the interface binding site and **6c** at the allosteric site and illustrated in SI1). Based on the interaction pattern and binding energy of **6c** and FBP, we concluded that the designed molecule **6c** has a lower affinity towards the allosteric binding site than FBP. On the other hand, binding energies of **6c** and FBP at the interface site were −64.2 and −30.7 Kcal/mol, respectively. The synthesized molecule **6c** showed multiple H-bonding, π-π stacking, and many unspecific hydrophobic interactions that correlate with their binding energies, as illustrated in Fig. 8. Overall, the affinity of **6c** is much higher at the interface binding site compared to the allosteric site. Therefore, its binding is independent of possible mutations at the FBP binding site that inhibit FBP binding and consequently hinder the tetramerization process. Furthermore, multiple simulations with the designed molecule **6c**, its variant **6c-OH** and FBP were performed and are discussed below to confirm that our designed molecules (**6c** and **6c-OH**) are capable of inducing the necessary conformational changes in the protein structure (PKM2) to drag the system towards tetramer (active) formation.

To identify the possible binding site of our molecule **6c** with PKM2, we evaluated two different binding sites in the dimeric state of the PKM2 using the docking protocol discussed in the method section. Our result suggested a lower binding affinity of **6c** at the allosteric binding site compared with the interface site. We performed docking in the monomeric, dimeric, and tetrameric states (data are shown). However, the best binding mode was observed at the dimeric state where **6c** binds at the monomeric interface site (between both monomers) as illustrated in Fig. 8. Similar binding modes for other molecules were also reported for PKM2.[50,51] At the monomeric interface, our molecule interacts with both the protein chains. This offered extra stability to the monomeric interface but also stabilizes the dimeric interface and supports the initiation of the tetramer formation process as discussed in the following section. We monitored the stability of interactions formed by PKM2 residues with **6c** during the course of MD simulations. Residues forming stable interactions with **6c** are displayed in Figure SI2. The binding pocket consists of hydrophobic and hydrophilic residues. Notably, **6c** formed many new interactions that were not present after the docking in the crystal structure. Polar groups of Asp354, Lys311, and Tyr391 interact with the polar moiety of **6c** while the hydrophobic segment of **6c** makes contact with Leu353, Ala388, and Tyr391. Herein, we have only considered the residues which maintained contacts or H-bonds for a significant fraction of the simulation time. We also observed some further interactions, but they formed only transiently and are therefore not reported here. We expect that combinations of such polar and hydrophobic contacts make the ligand–protein (**6c**-PKM2) binding more specific and possibly reduce binding to the other PK isoforms.

Proposed mechanism of tetramer formation: Experimental results demonstrated that our designed molecule **6c** drags the system towards tetramer formation even in the absence of natural allosteric ligand FBP. To understand the molecular mechanism of tetramer formation, we performed multiple simulations in the presence and absence of **6c** and FBP ligands as discussed in the method section. During the MD simulation of PKM2 dimer in the apo (without any ligand/FBP) and complex form, stability at the dimeric interface was closely monitored. Resultant root means square deviation (RMSD) time plots are illustrated in Fig. 9. A central dimeric interface was defined by selecting protein residues within 1.5 nm of the bound ligand (**6c**). RMSD plots (upper panel of Fig. 9) clearly demonstrate that in the presence of **6c** the central tetramer interface (magenta helices) is significantly stabilized compared with the apo simulation. Although this effect is most prominent in one of the simulations, other simulations showed transient interface stabilization. It is important to mention that we do not have a fully optimized force field for boronic acid. The Lennard Jones (LJ) parameters used by ATB for Boron corresponded to carbon and were not optimized separately. Therefore, we have also performed the docking and subsequent simulation of **6c-OH** molecule (Fig. SI3), which has similar LJ parameters to boron and is the most likely metabolite of **6c** formed after its

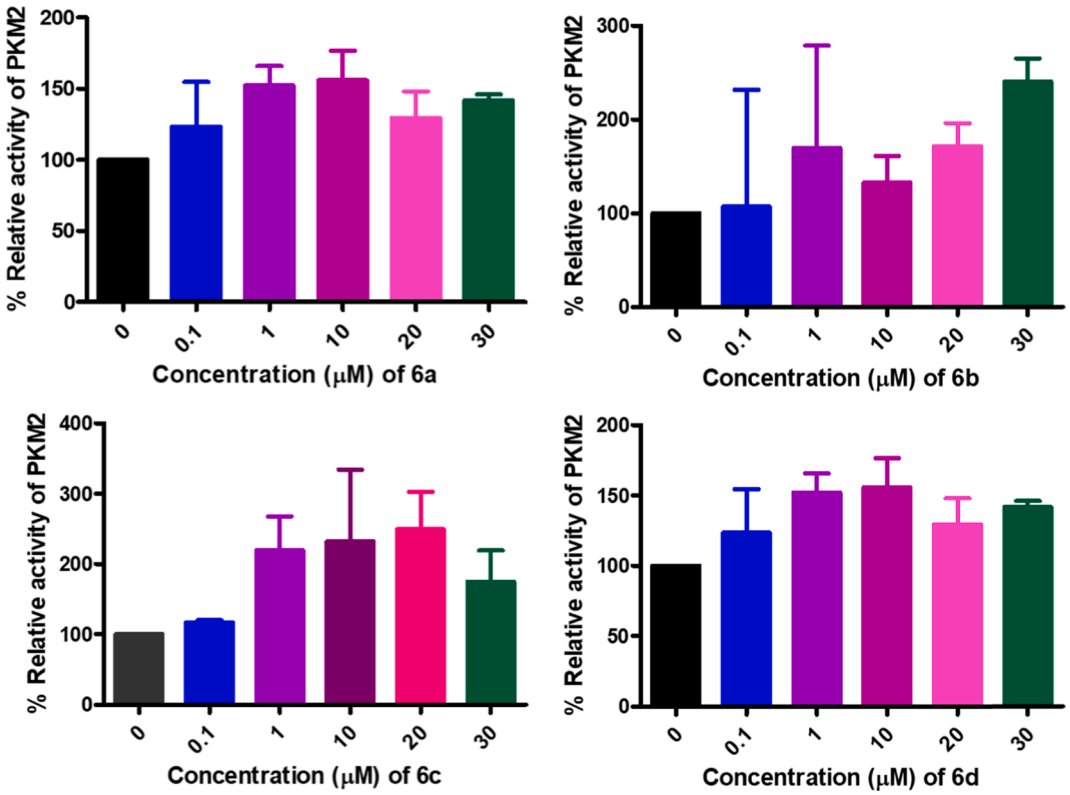

Fig. 5. % Relative pyruvate kinase activity of synthesized molecules (**6a-6d**) was determined using LDH-coupled enzyme assay. The reaction mixture contains (50 mM Tris-HCl (pH 7.5), 100 mM KCl, 10 mM $MgCl_2$, 0.6 mM PEP, 0.9 mM ADP, 0.12 mM β NADH and 4.8 U/ml LDH). Pyruvate kinase activity was measured at 25 °C by changing the absorbance of β NADH at 340 nm from 0 to 20 min.

Table 1
Relative cell growth inhibition of 6a-6d in various cancer cell lines.[a]

Compound Code	IC_{50} Value (μM)				
	Colo-201	BCL-2 Jurkat	MCF-7	MSCs	MDA-MB-231
6a	2.81 ± 0.12	6.36 ± 0.15	1.5 ± 0.32	40.6 ± 1.21	38.03 ± 0.33
6b	5.58 ± 0.45	0.09 ± 0.29	2.71 ± 0.37	29.43 ± 5.91	36.6 ± 3.59
6c	3.75 ± 0.47	2.82 ± 0.07	0.08 ± 0.24	23.86 ± 0.43	34.85 ± 1.59
6d	5.50 ± 0.03	0.57 ± 0.16	2.72 ± 0.12	25.83 ± 3.18	58.7 ± 9.02
Doxorubicin	0.80 ± 0.40	3.03 ± 0.18	1.08 ± 0.28	2.37 ± 0.80	1.30 ± 0.60

[a] MCF-7, breast cancer cell; COLO-201, colorectal adenocarcinoma cells; BCL-2Jurkat cells, Human Leukemia cells; MDA-MB-231, Triple-negative breast cancer cells ; MSCs, Mesenchymal Stem Cells.

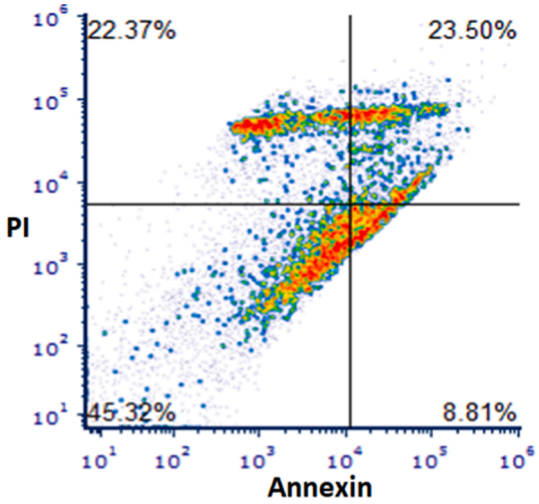

Fig. 6. Flow cytometric analysis of **6c** in the MCF-7 cell line after 48 h of drug treatment. PI: Propidium Iodide.

hydrolysis (Fig. 3).[52] As **6c-OH** does not contain the boron atom, its force field is accurately parameterized using ATP. The PKM2 dimer in the presence of **6c-OH** showed a stabilizing effect at the central dimer interface, illustrated by the blue color line in Fig. 9 upper panel. In contrast, the PKM2-FBP complex exhibits a totally different picture. We were expecting the bound FBP will significantly stabilize the tetramer interface, an advantage to tetramer formation. However, the PKM2-FBP complex displayed the highest RMSD value (up to 0.33 nm) at the central dimeric interface. We have also monitored the RMSD value at the terminal dimer interface (magenta and yellow color secondary structures) as depicted in Fig. 9 lower panel to solve this mystery. FBP has two binding sites, one at each monomer, compared with only one binding site for our ligands (at the monomer interface). Therefore, we have monitored the effect at both FBP binding sites separately. We have observed significantly lower RMSD values at both sites compared with the apo form (Fig. 9 lower panel and Fig. SI4). The Apo form displayed an average RMSD value of ~ 0.3 nm compared with an average of ~ 0.21 nm observed in the PKM2-FBP complexes, as illustrated in Fig. 9. Based on the above-mentioned results, we proposed the following model for the tetramer formation process. Both **6c**, **6c-OH,** and **FBP** drag the dimeric (PKM2) system towards tetramerization via slightly different mechanisms. **6c** and **6c-OH** stabilized the central dimeric interface and possibly trigger the tetramer formation process from there. It was shown previously[50,51] that this interface contains key residues that are critical

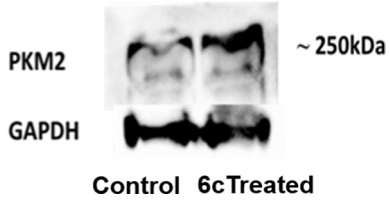

Fig. 7. MCF-7 cells were treated with 100 nM of **6c** for 48 h. **6c** treated cells are showing more tetramer compared to untreated cells (control). Disuccinimidyl suberate (DSS) cross-linker assay ascertains tetramer expression of the PKM2 in MCF-7 cell line on SDS-PAGE.

to initiate the tetramer formation process.

Therefore, the stability of this interface is crucial for tetramer formation. Contrarily, the mode of action of FBP is very different. The binding of FBP stabilizes the terminal dimeric interfaces at both sides. The tetramer formation process possibly initiates from this location. The different binding sites and distinct mechanisms further suggest that our molecules are independent of FBP binding. The study suggests that in mutant proteins where FBP cannot bind to the monomers, our molecule alone is able to drag the system towards tetramer formation. Such *in-silico* mutants and their effect on the tetramer formation process need to be further analyzed.

Further, gastro-retentive tablets of **6c** were prepared to check its efficacy in the *ex vivo* model. The idea stemmed from the fact that fecal tumor PKM2 is a highly sensitive marker for colorectal cancer (CRC) which is the third most prevalent cancer in the world.[53,54] PKM2 also correlates with more advanced stages of CRC, and its reduction is associated with successful surgical intervention. 5-Fluoro uracil (5-FU), oxaliplatin, and irinotecan are chiefly employed for parenteral chemotherapy of CRC. In recent years a number of cytotoxic drugs such as capecitabine, vinorelbine, or topotecan have been developed as oral agents for the parenteral treatment of colon cancer.[55] However, to target the CRC with an orally bioavailable molecule, appropriate release profile and mucoadhesion are vital parameters for sustained release in the colon.[56] To address the challenge a sustained release formulation was designed. The physicochemical evaluation of the compound was determined, wherein the molecule was found to be lipophilic in nature, making it unfavorable for oral administration. The molecule **6c** was bioactive but lacked suitable pharmaceutical properties. Therefore, the development of an orally bioavailable form of **6c** was undertaken. Excellent solubility and satisfactory dissolution rate are essential conditions for the clinical applications of candidate drugs.[57–59] For this purpose, we selected thiolated chitosan nanoparticles that show mucoadhesive properties leading to the release of drug at the colonic mucosal surface.[60]

Zeta sizer measures the size of the particle-based on its light scattering ability.[61] Smaller the particle, less is the scattering and more scattering for larger particles. After treatment with **6c**, PKM2 protein is

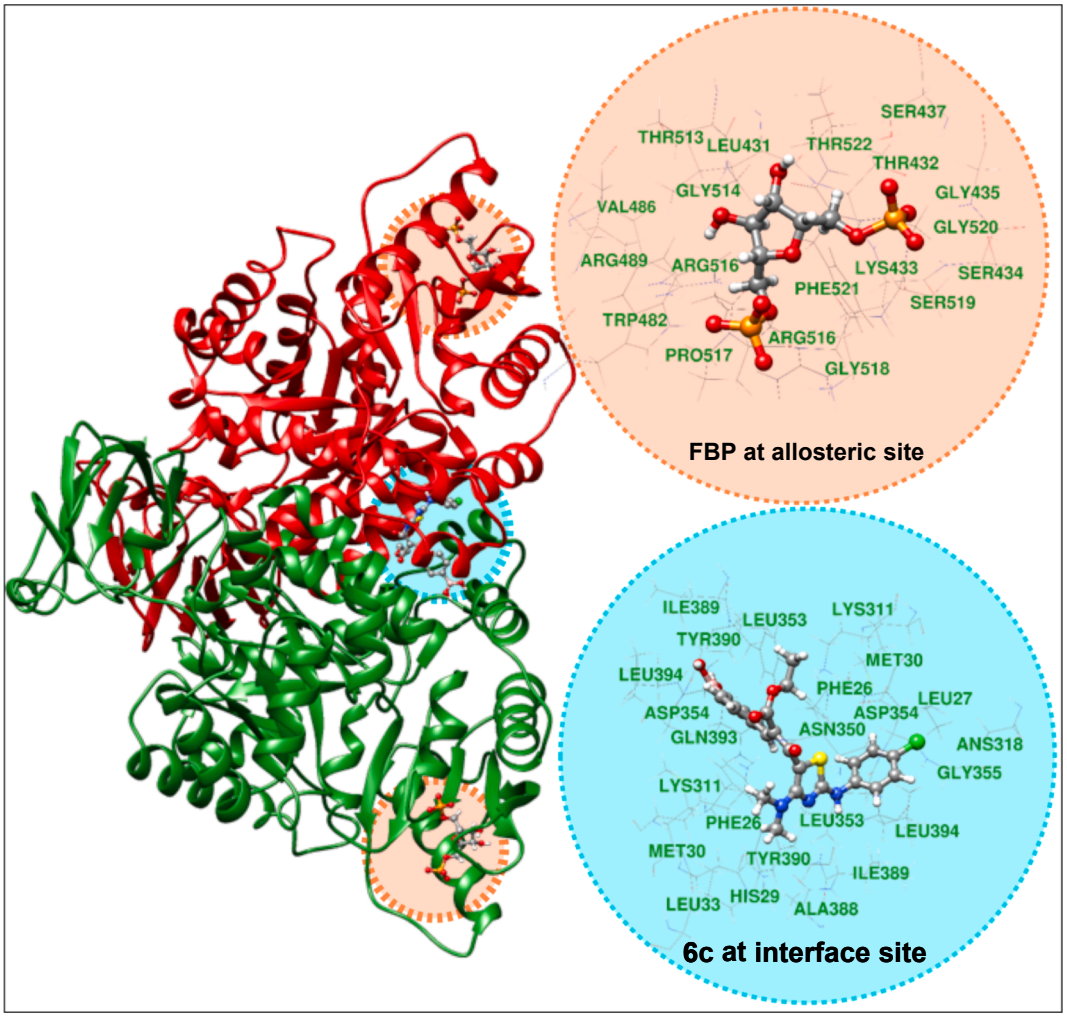

Fig. 8. Docked protein–ligand complex in the PKM2 dimeric state with **6c** at interface binding site (cyan) and with FBP at an allosteric site (orange). Monomeric chains A and C are colored in red and green, respectively. Ligands were shown in ball and stick representations, while protein residues were displayed in the wireframe. Carbon, nitrogen, oxygen, sulfur, fluorine, hydrogen, and boron were colored in grey, blue, red, yellow, green, white, and pink colors, respectively.

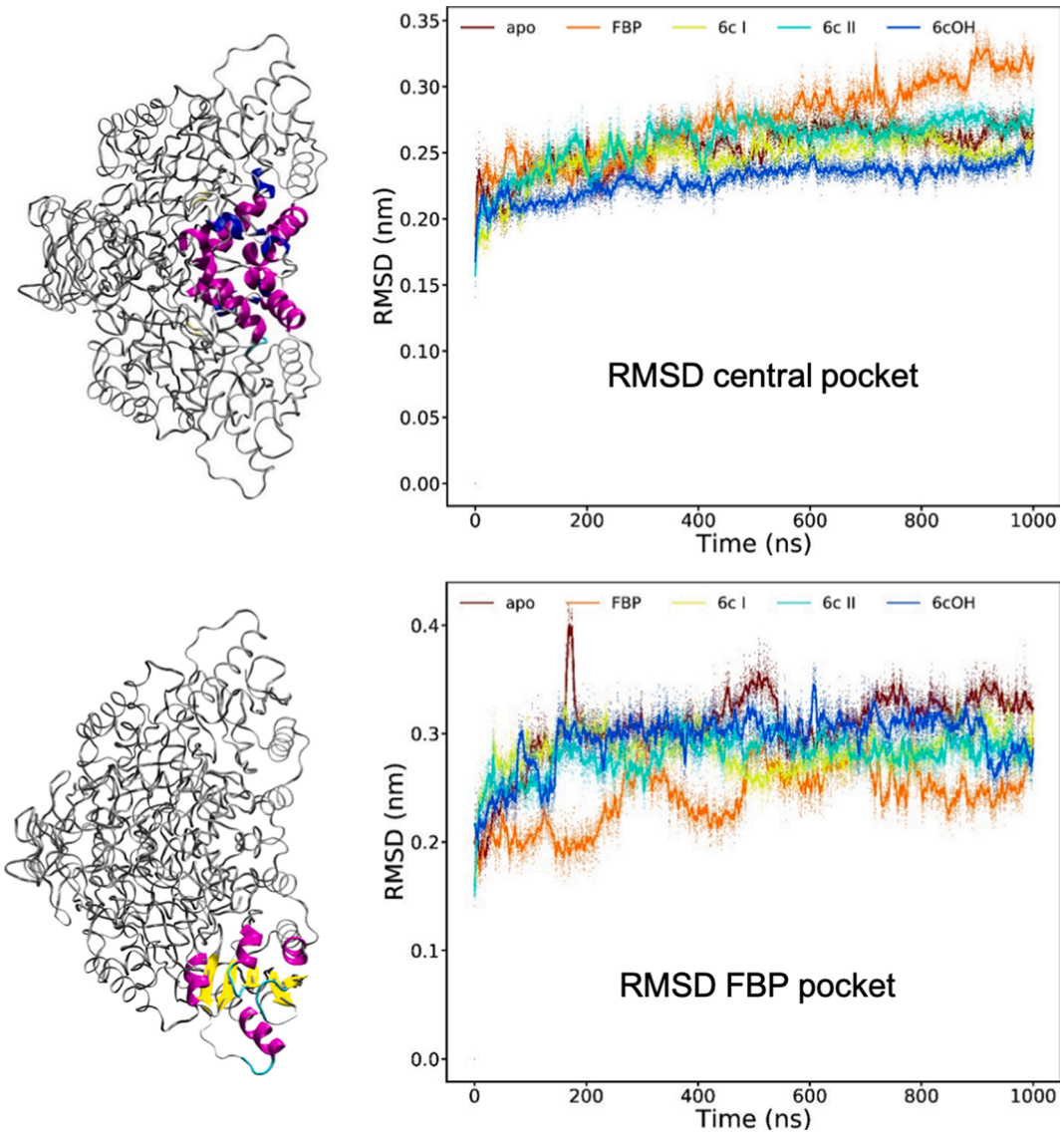

Fig. 9. RMSD values of the central pocket (upper panel) and FBP pocket (lower panel). Part of the protein that forms the central pocket is shown in magenta/blue color in the upper left panel. FBP pocket is illustrated in the magenta/yellow color in the lower-left panel. **6c** I and **6c** II represent the data from two independent simulations.

expected to tetramerize. Due to which its molecular size will increase and hence the scattering too. Scattering observed by DLS was doubled after treatment with the compound **6c** (Fig. 10).

First, thiolated chitosan was synthesized following the protocol described earlier with appropriate modifications.[59] The hydrodynamic particle size and zeta potential of the NPs were monitored by optimizing the ratio of TPP and thiolated chitosan. Finally, 3:1 (S-Ch: TPP) weight ratio was used to prepare NPs. The average hydrodynamic particle size of S-Ch NPs was found to be 130.42 ± 3.2 nm, and the zeta potential was 20.92 ± 2.13 mV (Fig. 11A and 11B). Being polysaccharides in nature

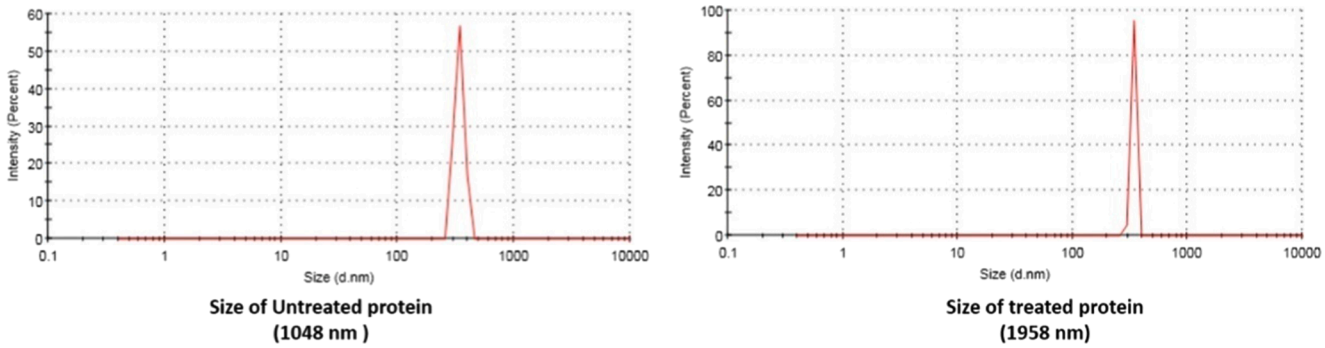

Fig. 10. Dynamic Light Scattering (DLS) of PKM2 before treatment (left) with **6c** and after (right) treatment with **6c**.

chitosan-based NPs formed via cross-linking, exhibited minimal energy in the dispersion when they are in the form of NPs.

NPs were monitored by optimizing the ratio of TPP and thiolated chitosan. Finally, 3:1 (S-Ch: TPP) weight ratio was used to prepare NPs. The average hydrodynamic particle size of S-Ch NPs was 130.42 ± 3.2 nm, and the zeta potential was 20.92 ± 2.13 mV (Fig. 11A and B). Being polysaccharides in nature chitosan-based NPs formed via cross-linking exhibited minimal energy in the dispersion when they are in the form of NPs. Further, mucin, S-Ch-NPs, and mucin + S-Ch-NPs were tested for zeta potential to observe the binding of S-Ch-NPs with mucin. Formulation with the experiment was carried out by treating different formulations with excised goat intestinal segment. As shown in Fig. 11D zeta potential of mucin was changed after the addition of the S-Ch-NPs indicating that it possesses an affinity for the mucin present in the mucous layer of the intestine where **6c** is destined to act. The entrapment efficiency (EE) indicates the compound's can be successfully entrapped into NPs.[62] The EE of the S-Ch NPs + **6c** was determined with an indirect method after isolation of NPs by centrifuging them. The EE of S-Ch-NPs + 6c was found to be 73.63 ± 1.21%. This high EE might originate from the tendency of **6c** to enter the core of the S-Ch-NPs. The DL of S-Ch-NPs + **6c** was found to be 30.21 ± 2.1% which might be due to the hydrophilic nature of the S-Ch.[63]

Apart from formulation composition, drug release profile may be another important factor that must be appropriately considered to obtain required anticancer activity from the developed formulation.[64] The *in vitro* release profile of the **6c**-loaded **S-Ch-NPs** is shown in Fig. 12. It shows a controlled release profile, suggesting that the **S-Ch-NPs** acts as a barrier against the release of entrapped drugs from the polymeric matrix into the release medium.

Moreover, the release data, when fitted into different kinetic models viz zero order, first order, Hixon Rowell and Higuchi value of the coefficient of correlation (r^2) was calculated by linear regression analysis using graph pad InStat software to evaluate the accuracy of the fit.[65] *In vitro* drug release was evaluated in three different media using USP Dissolution apparatus II. The test started with pH 1.5 HCl buffer

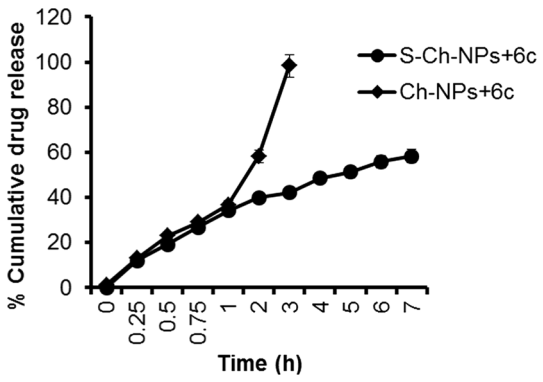

Fig. 12. *In vitro* drug release profile from S-Ch-NP + **6c** and Ch-NP + **6c** formulations.

followed by replacement with phosphate buffer (pH 6.8) for 4 and subsequent replacement with phosphate buffer (pH 7.4) with a total duration of 12 h. Results are represented as mean ± SD (n = 3). The zero-order kinetics indicated an initial rapid release of **6c** from the S-Ch-NPs followed by a slow zero-order and regression value of 0.9975 (Fig. SI6). The fitting of the first-order release kinetics model led to a regression value of 0.7145, signifying that the formulation does not follow a first-order release pattern. The Higuchi matrix model regression was found to be 0.6775, whereas the Hixson Crowell release shows a regression of 0.6639. By calculating and comparing r^2 value for all models, zero-order release was found to be the best fit model, which suggests that the drug was released at a particular site in a sustained manner. The zero-order kinetic model was found suitable for the release of drugs from the S-Ch-NPs, which might be due to a barrier property of chitosan to the release of **6c**.[66,67] Fig. 13A and B indicates that the applied force is directly proportional to the detachment force and work of adhesion. When applied force was increased, the required detachment force for sample disc from intestinal mucosa also increased, indicating the greater

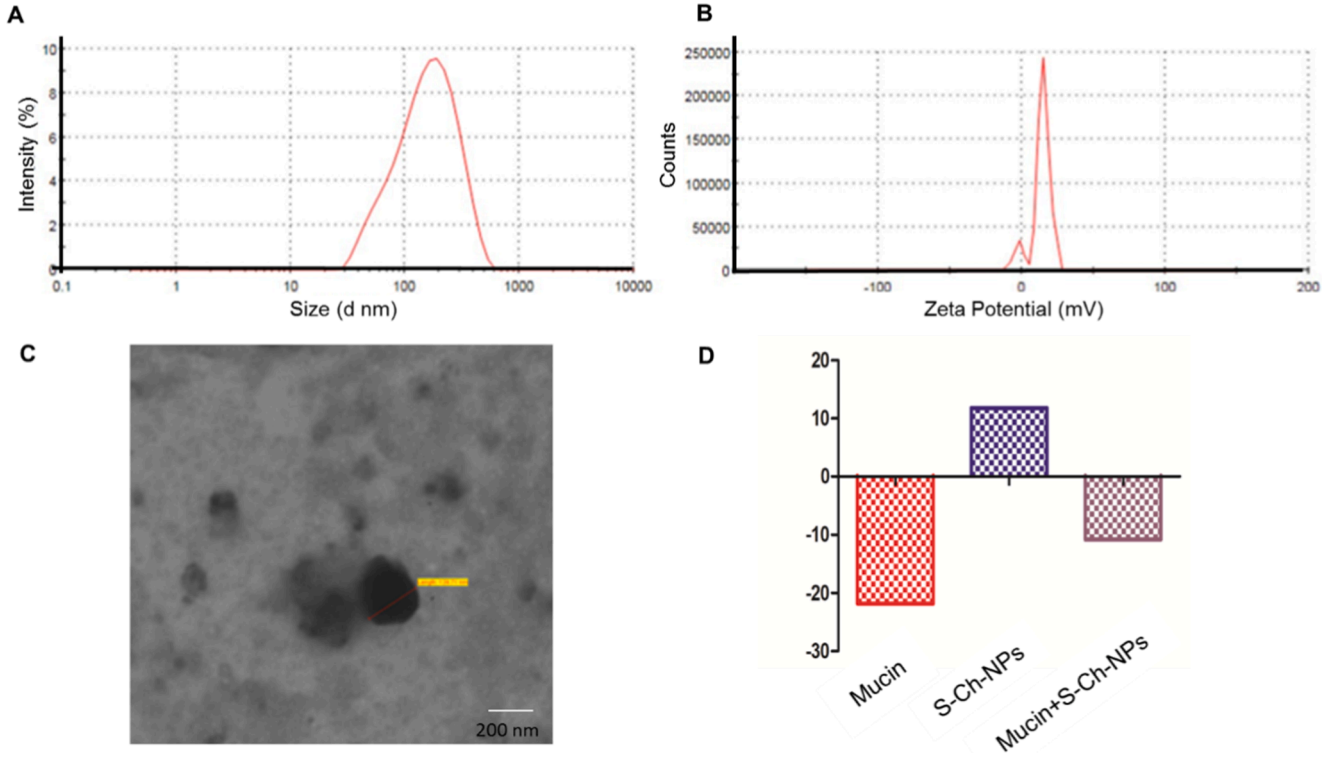

Fig. 11. A. Average size of S-Ch-NPs_**6c B**. Zeta potential of S-Ch-NPs_**6c. C**. Surface morphology using scanning electron microscope. **D**. Change in the zeta potential of tested formulation to predict binding with mucin. Nanoparticles-Ch-NPs + **6c**.

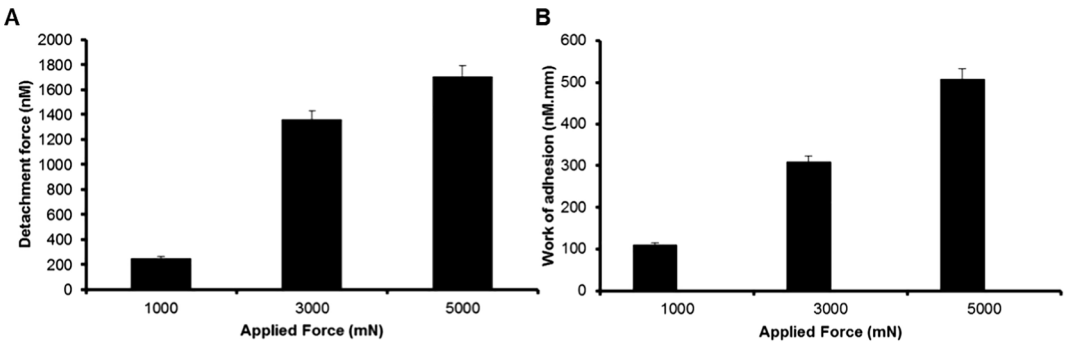

C

Time (h)	In vitro Dissolution (%)	
	Ch-NPs+6c tablets	S-Ch-NPs+6c tablets
0	0±0.0	0±0.0
1	4±0.7	3±0.5
2	7±0.9	6±0.6
3	10±1.2	9±1.1
4	26±1.4	15±1.3
5	41±1.9	28±1.8
6	59±2.6	36±1.9
7	71±3.9	44±2.7
8	89±4.8	54±2.9
9	96±3.9	61±3.4
10	-	67±4.6
11	-	73±5.1
12	-	79±5.2

Fig. 13. **A**. Effect of applied force on the detachment of sample disc from goat intestinal mucosa. **B**. Effect of different applied force on the work of adhesion (area under the curve). **C.** *In vitro* dissolution investigation of Ch-NPs + 6c and S-Ch-NPs + 6c tablets determined in a different medium to simulate GIT pH from stomach to lower intestine (colon).

mucoadhesive potential of the synthesized compound. The same phenomenon was observed with the work of adhesion, as increased applied force showed maximum work of adhesion. The applied force of 5000 mN showed maximum detachment force and work of adhesion, i. e. 1707.21 mN and 507.42 mN respectively. The further increased applied force showed rupture of the intestinal mucosa.

Characterization of S-Ch-NPs + 6c gastroretentive tablets

Plain tablets (without thiolated chitosan) and tablets containing **6c** entrapped S-Ch-NPs were prepared successfully employing direct compression method using microcrystalline cellulose as filler, magnesium stearate, and Cab-O-Sil as a lubricant and cellulose acetate phthalate as enteric coating polymer.[68,69] The developed core tablets had a smooth surface, with hardness ranging from 3 ± 1 kg (500 mg tablet). Moreover, in the weight variation test, randomly selected 20 tablets were weighed individually, and the average weight was found to be 500 ± 6.72 mg. Evaluated tablet parameters are shown in Table S16 and comply with standard pharmacopoeial limits.

Dissolution data showed that Ch-NPs + 6c tablets released ~ 90% of **6c** in 8 h, while ~ 79% of **6c** was found released from S-Ch-NPs + **6c** tablets. As shown in Fig. 13C, the release pattern was identical till 3 h due to the presence of enteric polymer. Afterward, **6c** was released at a faster rate from Ch-NPs + **6c** tablets compared to S-Ch-NPs + **6c** tablets attributed to the presence of thiolated chitosan. Besides, less than 10% of **6c** was released in either case and therefore comply with standard pharmacopeial limits. Conclusively, the S-Ch-NP + **6c** tablet provides sustained drug release and it was found that 79.12 ± 5.2% of **6c** was released within 12 h. It also explains why the release was slower at this pH compared to that at pH 1.5. Similarly, the **6c** formulation showed antiproliferative activity as compared to **6c** (Fig. SI5). Protein cross-linking assay indicates that **6c** based nanoformulation converts dimeric PKM2 into the tetrameric form of PKM2 (Fig. 14).

Cancer cells anchorage genetic changes that escalate nutrient uptake and alter their metabolism to support anabolic processes to activate alternate metabolic pathways. Interfering with this metabolic program is a strategy for cancer therapy. Altered glucose metabolism is common in cancer cells and is mediated in part by the expression of PKM2 that acts as metabolic bug with distinct regulatory properties. FBP

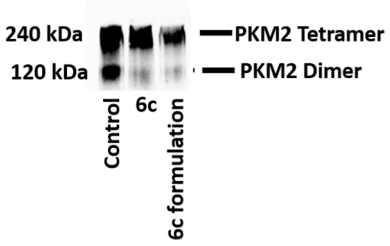

Fig. 14. Tetramer formation of PKM2 in MCF-7 cell line on SDS-PAGE. MCF-7 cells were treated with 100 nM of **6c** for 48 h. Disuccinimidyl suberate (DSS) cross-linker assay ascertains conversion of PKM2 dimeric form to tetrameric form.

allosterically activates PKM2. It is found to interact with tyrosine-phosphorylated proteins, resulting in the release of FBP, leading to decreased enzyme activity. Hence activation of PKM2 might resist and interfere with the Warburg effect.

In accordance with the same line of thought, our data show that high pyruvate kinase activity caused by boronic acid-based small-molecule PKM2 activation slows down the ability of cancer cells to divide with limitless replicative potential. Several recent publications have described activators and inhibitors of PKM2. These range from judiciously designed drug-like molecules to several polyphenols having poor developability owing to the propensity of PAINS (Pan assay interference compounds). Although several of these PKM2 modulators may prevent tumor cell proliferation, our data suggest that judiciously designed boronic acid derivatives can activate PKM2 enzyme and cancerous cells can be efficiently challenged with designed ligands.

It is known that small-molecules like DASA-58 and ML-265 can activate PKM2 and can also alter cell metabolism, but they are yet to hit the market. Therefore, novel agents targeting this enzyme must be readily developed to be given alone or in combination with available therapeutics. Our studies focused on boronic acid-based ligands, which are representative of PKM2-activating compounds. These small molecules (**6a-6d**) modified the kinetic properties of PKM2 analogous to those induced by FBP. Astonishingly, computational analyses of the activators bound to PKM2 tetramers revealed a binding pocket at the interface of the subunit interaction that is distinct from the site of FBP or PEP binding. Unlike FBP, which stabilizes the C—C′ interface of the active tetramer, the boronic acid-based activators stabilized the central dimer interface. It is also proposed elsewhere that under *in vivo* environment, much of the PKM2 exists in an equilibrium between loosely associated tetramers having low activity and tightly associated tetramers having high activity. This equilibrium is influenced by concentrations of FBP. The simulation studies also demonstrated the role of developed ligand **6c** in facilitating tetramer formation.

Our findings are consistent with our hypothesis, our data showed that PKM2 activation caused by rationally designed boronic acid-based molecules impedes the ability of cancer cells to divide and proliferate indiscriminately. **6c** localization at the colon area was achieved by preparing enteric-coated gastroretentive tablets composed of thiolated chitosan NPs as they could be delivered directly to large bowel. Enteric coating helps in preventing the degradation of the active molecule at gastric pH. The S-Ch-NPs + **6c** mediated tablets represent a potential drug delivery approach for effective delivery of the **6c** to the colorectal tumors. Compound **6c** was found to be highly potent across several cell lines and was chosen. Out of four molecules synthesized, **6c** exerted specific cytotoxicity against colon cancer cells with a hyperactive PKM2. Further to drag the compound specifically towards colon cells, nano-formulation was developed, and it was found that **6c** exhibited improved pharmacokinetic properties. The study strongly suggested that the lead developed as formulation may offer a novel and targeted treatment option for human colorectal cancer. Although our data indicate that small-molecule activation of PKM2 can impede the proliferation of cancer cells *in vitro*, it remains to be determined whether such compounds will be similarly effective in autochthonous or xenograft mouse tumor models or will be efficacious as a cancer therapy in humans.

Declaration of Competing Interest

The authors declare that they have no known competing financial interests or personal relationships that could have appeared to influence the work reported in this paper.

Acknowledgements

This research was supported by the National Institute of Pharmaceutical Education and Research-Ahmedabad, Department of Pharmaceuticals, Ministry of Chemicals and Fertilizers, Government of India. The authors gratefully acknowledge Prof. Kiran Kalia, Director, NIPER-Ahmedabad, for her motivation and constant support throughout the project. The communication number for this manuscript is NIPER-A/344/09/2019.

Appendix A. Supplementary data

Supplementary data to this article can be found online at https://doi.org/10.1016/j.bmcl.2021.128062.

References

1 Israelsen WJ, Vander Heiden MG. Pyruvate kinase: function, regulation and role in cancer. *Semin Cell Dev Biol.* 2015;43:43–51. https://doi.org/10.1016/j.semcdb.2015.08.004.
2 Kumar S, Barth A. Phosphoenolpyruvate and Mg2+ binding to pyruvate kinase monitored by infrared spectroscopy. *Biophys J.* 2010;98:1931–1940. https://doi.org/10.1016/j.bpj.2009.12.4335.
3 Osterman J, Fritz PJ, Wuntch T. Pyruvate kinase isozymes from rat tissues developmental studies. *J Biol Chem.* 1973;248:1011–1018. https://doi.org/10.1016/S0021-9258(19)44364-0.
4 Wu S, Le H. Dual roles of PKM2 in cancer metabolism. *Acta Biochim Biophys Sin.* 2013;45:27–35. https://doi.org/10.1093/abbs/gms106.
5 Guo C, Li G, Hou J, et al. Tumor pyruvate kinase M2: a promising molecular target of gastrointestinal cancer. *Chinese J Cancer Res.* 2018;30:669. https://doi.org/10.21147/j.issn.1000-9604.2018.06.11.
6 Yang J, Liu H, Liu X, Gu C, Luo R, Chen H-F. Synergistic allosteric mechanism of fructose-1, 6-bisphosphate and serine for pyruvate kinase M2 via dynamics fluctuation network analysis. *J Chem Inf Model.* 2016;56:1184–1192. https://doi.org/10.1021/acs.jcim.6b00115.
7 Prakasam G, Iqbal MA, Bamezai RNK, Mazurek S. Posttranslational modifications of pyruvate kinase M2: tweaks that benefit cancer. *Front Oncol.* 2018;8:22. https://doi.org/10.3389/fonc.2018.00022.
8 Warner SL, Carpenter KJ, Bearss DJ. Activators of PKM2 in cancer metabolism. *Future Med Chem.* 2014;6:1167–1178. https://doi.org/10.4155/fmc.14.70.
9 Alves-Filho JC, Pålsson-McDermott EM. Pyruvate kinase M2: a potential target for regulating inflammation. *Front Immunol.* 2016;7:145. https://doi.org/10.3389/fimmu.2016.00145.
10 Jiang J, Walsh MJ, Brimacombe KR, et al. *ML265: A potent PKM2 activator induces tetramerization and reduces tumor formation and size in a mouse xenograft model. Probe Reports from the NIH Molecular Libraries Program [Internet].* National Center for Biotechnology Information (US); 2013. https://www.ncbi.nlm.nih.gov/books/NBK153222/.
11 Li J, Li S, Guo J, et al. Natural product micheliolide (MCL) irreversibly activates pyruvate kinase M2 and suppresses leukemia. *J Med Chem.* 2018;61:4155–4164. https://doi.org/10.1021/acs.jmedchem.8b00241.
12 Keller KE, Doctor ZM, Dwyer ZW, Lee Y-S. SAICAR induces protein kinase activity of PKM2 that is necessary for sustained proliferative signaling of cancer cells. *Mol Cell.* 2014;53:700–709. https://doi.org/10.1016/j.molcel.2014.02.015.
13 Chaikuad A, Koch P, Laufer SA, Knapp S. The cysteinome of protein kinases as a target in drug development. *Angew Chemie Int Ed.* 2018;57:4372–4385. https://doi.org/10.1002/anie.201707875.
14 Anastasiou D, Yu Y, Israelsen WJ, et al. Pyruvate kinase M2 activators promote tetramer formation and suppress tumorigenesis. *Nat Chem Biol.* 2012;8:839–847. https://doi.org/10.1038/nchembio.1060.
15 Hsieh I-S, Gopula B, Chou C-C, et al. Development of novel irreversible pyruvate kinase M2 inhibitors. *J Med Chem.* 2019;62:8497–8510. https://doi.org/10.1021/acs.jmedchem.9b00763.
16 Ricci F, Vallée-Bélisle A, Porchetta A, Plaxco KW. Rational design of allosteric inhibitors and activators using the population-shift model: in vitro validation and application to an artificial biosensor. *J Am Chem Soc.* 2012;134:15177–15180. https://doi.org/10.1021/ja304672h.
17 Albers HMHG, van Meeteren LA, Egan DA, van Tilburg EW, Moolenaar WH, Ovaa H. Discovery and optimization of boronic acid based inhibitors of autotaxin. *J Med Chem.* 2010;53:4958–4967. https://doi.org/10.1021/jm1005012.
18 Parrill AL, Baker DL. Autotaxin inhibitors: a perspective on initial medicinal chemistry efforts. *Expert Opin Ther Pat.* 2010;20:1619–1625. https://doi.org/10.1517/13543776.2010.533658.
19 Lienhard GE, Koehler KA. 2-phenylethaneboronic acid, a possible transition-state analog for chymotrypsin. *Biochemistry.* 1971;10:2477–2483. https://doi.org/10.1021/bi00789a008.
20 Whyte GF, Vilar R, Woscholski R. Molecular recognition with boronic acids—applications in chemical biology. *J Chem Biol.* 2013;6:161–174. https://doi.org/10.1007/s12154-013-0099-0.
21 Trippier PC, McGuigan C. Boronic acids in medicinal chemistry: anticancer, antibacterial and antiviral applications. *Medchemcomm.* 2010;1:183–198. https://doi.org/10.1039/C0MD00119H.
22 Field-Smith A, Morgan GJ, Davies FE. Bortezomib (Velcade™) in the treatment of multiple myeloma. *Ther Clin Risk Manag.* 2006;2:271–279. https://doi.org/10.2147/tcrm.2006.2.3.271.

23 Kong Y, Grembecka J, Edler MC, et al. Structure-based discovery of a boronic acid bioisostere of combretastatin A-4. *Chem Biol*. 2005;12:1007–1014. https://doi.org/10.1016/j.chembiol.2005.06.016.

24 Issa F, Kassiou M, Rendina LM. Boron in drug discovery: carboranes as unique pharmacophores in biologically active compounds. *Chem Rev*. 2011;111:5701–5722. https://doi.org/10.1021/cr2000866.

25 Wang L, Xie S, Ma L, Chen Y, Lu W. 10-Boronic acid substituted camptothecin as prodrug of SN-38. *Eur J Med Chem*. 2016;116:84–89. https://doi.org/10.1016/j.ejmech.2016.03.063.

26 Lee CF, Diaz DB, Holownia A, et al. Amine hemilability enables boron to mechanistically resemble either hydride or proton. *Nat Chem*. 2018;10:1062–1070. https://doi.org/10.1038/s41557-018-0097-5.

27 Das J, Chen P, Norris D, et al. 2-Aminothiazole as a novel kinase inhibitor template. Structure− activity relationship studies toward the discovery of N-(2-chloro-6-methylphenyl)-2-[[6-[4-(2-hydroxyethyl)-1-piperazinyl)]-2-methyl-4-pyrimidinyl] amino)]-1, 3-thiazole-5-carboxamide (Dasatinib, BMS-354825) as a Potent *pan*-Src Kinase Inhibitor. *J Med Chem*. 2006;49:6819–6832. https://doi.org/10.1021/jm060727j.

28 Bestgen B, Krimm I, Kufareva I, et al. 2-Aminothiazole derivatives as selective allosteric modulators of the protein kinase CK2. 1. Identification of an allosteric binding site. *J Med Chem*. 2019;62:1803–1816. https://doi.org/10.1021/acs.jmedchem.8b01766.

29 Müller G. Medicinal chemistry of target family-directed masterkeys. *Drug Discov Today*. 2003;8:681–691. https://doi.org/10.1016/S1359-6446(03)02781-8.

30 Gulbake A, Jain A, Jain A, Jain A, Jain SK. Insight to drug delivery aspects for colorectal cancer. *World J Gastroenterol*. 2016;22:582–599. https://doi.org/10.3748/wjg.v22.i2.582.

31 Zagade AD, Shard A, Shinde S, Sahu AK, Sengupta P. Bioanalysis and quadrupole-time of flight-mass spectrometry driven in vitro metabolite profiling of a new boronic acid-based anticancer molecule. *J Chromatogr Sci*. 2020;58:796–803. https://doi.org/10.1093/chromsci/bmaa044.

32 Patel S, Patle R, Parameswaran P, Jain A, Shard A. Design, computational studies, synthesis and biological evaluation of thiazole-based molecules as anticancer agents. *Eur J Pharm Sci*. 2019;134:20–30. https://doi.org/10.1016/j.ejps.2019.04.005.

33 Siddiqui FA, Prakasam G, Chattopadhyay S, et al. Curcumin decreases Warburg effect in cancer cells by down-regulating pyruvate kinase M2 via mTOR-HIF1α inhibition. *Sci Rep*. 2018;8:1–9. https://doi.org/10.1038/s41598-018-25524-3.

34 Yoon YJ, Kim Y-H, Jin Y, et al. 2′-hydroxycinnamaldehyde inhibits cancer cell proliferation and tumor growth by targeting the pyruvate kinase M2. *Cancer Lett*. 2018;434:42–55. https://doi.org/10.1016/j.canlet.2018.07.015.

35 Dains FB, Brewster RQ, Olander CP. Phenyl isothiocyanate: isothiocyanic acid, phenyl ester. *Org Synth*. 2003;6:72. https://doi.org/10.1002/0471264180.os006.22.

36 Yavari I, Shahvelayati AS, Malekafzali A. Efficient synthesis of functionalized 2, 4-diaminothiazoles from tetramethylguanidine, isothiocyanates, and α-bromoketones. *J Sulfur Chem*. 2010;31:499–508. https://doi.org/10.1080/17415993.2010.525709.

37 Feng Y, Zou M, Song R, Shao X, Li Z, Qian X. Formation of 1, 4, 2-dithiazolidines or 1, 3-thiazetidines from 1, 1-dichloro-2-nitroethene and phenylthiourea derivatives. *J Org Chem*. 2016;81:10321–10327. https://doi.org/10.1021/acs.joc.6b01307.

38 Sharma N, Sharma A, Shard A, Kumar R, Sinha AK. Pd-catalyzed orthogonal Knoevenagel/Perkin condensation–decarboxylation–heck/suzuki sequences: tandem transformations of benzaldehydes into hydroxy-functionalized antidiabetic stilbene-cinnamoyl hybrids and asymmetric distyrylbenzenes. *Chem Eur J*. 2011;17:10350–10356. https://doi.org/10.1002/chem.201101174.

39 Boxer MB, Jiang J, Vander Heiden MG, et al. Evaluation of substituted N, N′-diarylsulfonamides as activators of the tumor cell specific M2 isoform of pyruvate kinase. *J Med Chem*. 2010;53:1048–1055. https://doi.org/10.1021/jm901577g.

40 Lin Y, Liu F, Fan Y, et al. Both high expression of pyruvate kinase M2 and vascular endothelial growth factor-C predicts poorer prognosis in human breast cancer. *Int J Clin Exp Pathol*. 2015;8:8028–8037. PMID: 26339369.

41 Liang J, Cao R, Wang X, et al. Mitochondrial PKM2 regulates oxidative stress-induced apoptosis by stabilizing Bcl2. *Cell Res*. 2017;27:329–351. https://doi.org/10.1038/cr.2016.159.

42 Berridge MV, Tan AS. Characterization of the cellular reduction of 3-(4, 5-dimethylthiazol-2-yl)-2, 5-diphenyltetrazolium bromide (MTT): subcellular localization, substrate dependence, and involvement of mitochondrial electron transport in MTT reduction. *Arch Biochem Biophys*. 1993;303:474–482. https://doi.org/10.1006/abbi.1993.1311.

43 He X, Du S, Lei T, et al. PKM2 in carcinogenesis and oncotherapy. *Oncotarget*. 2017;8:110656–110670. https://doi.org/10.18632/oncotarget.22529.

44 Peterson P, Whatcott CJ, Bearss DJ, Warner SL, Siddiqui-Jain A. Abstract B024: PKM2 activation suppresses cellular ROS scavenging capacity and potentiates doxorubicin antitumor activity; 2018. doi:10.1158/1535-7163.

45 Cortés-Cros M, Hemmerlin C, Ferretti S, et al. M2 isoform of pyruvate kinase is dispensable for tumor maintenance and growth. *Proc Natl Acad Sci*. 2013;110:489–494. https://doi.org/10.1073/pnas.1212780110.

46 Liberti MV, Locasale JW. The Warburg effect: how does it benefit cancer cells? *Trends Biochem Sci*. 2016;41:211–218. https://doi.org/10.1016/j.tibs.2015.12.001.

47 Wong N, De Melo J, Tang D. PKM2, a central point of regulation in cancer metabolism. *Int J Cell Biol*. 2013;2013. https://doi.org/10.1155/2013/242513.

48 Vander Heiden MG, Cantley LC, Thompson CB. Understanding the Warburg effect: the metabolic requirements of cell proliferation. *Science*. 2009;324:1029–1033. https://doi.org/10.1126/science.1160809.

49 Ding Y, Xue Q, Liu S, et al. Identification of parthenolide dimers as activators of pyruvate kinase M2 in xenografts of glioblastoma multiforme in vivo. *J Med Chem*. 2020;63:1597–1611. https://doi.org/10.1021/acs.jmedchem.9b01328.

50 Matsui Y, Yasumatsu I, Asahi T, et al. Discovery and structure-guided fragment-linking of 4-(2, 3-dichlorobenzoyl)-1-methyl-pyrrole-2-carboxamide as a pyruvate kinase M2 activator. *Bioorg Med Chem*. 2017;25:3540–3546. https://doi.org/10.1016/j.bmc.2017.05.004.

51 Dombrauckas JD, Santarsiero BD, Mesecar AD. Structural basis for tumor pyruvate kinase M2 allosteric regulation and catalysis. *Biochemistry*. 2005;44:9417–9429. https://doi.org/10.1021/bi0474923.

52 Boulanger E, Huang L, Rupakheti C, MacKerell Jr AD, Roux B. Optimized Lennard-Jones parameters for druglike small molecules. *J Chem Theory Comput*. 2018;14:3121–3131. https://doi.org/10.1021/acs.jctc.8b00172.

53 Aran V, Victorino AP, Thuler LC, Ferreira CG. Colorectal cancer: epidemiology, disease mechanisms and interventions to reduce onset and mortality. *Clin Colorectal Cancer*. 2016;15:195–203. https://doi.org/10.1016/j.clcc.2016.02.008.

54 Koss K, Maxton D, Jankowski JAZ. Faecal dimeric M2 pyruvate kinase in colorectal cancer and polyps correlates with tumour staging and surgical intervention. *Color Dis*. 2008;10:244–248. https://doi.org/10.1111/j.1463-1318.2007.01334.x.

55 Colomer R, Alba E, González-Martin A, et al. Treatment of cancer with oral drugs: a position statement by the Spanish Society of Medical Oncology (SEOM). *Ann Oncol*. 2010;21:195–198. https://doi.org/10.1093/annonc/mdp595.

56 Sharma S, Saltz LB. Oral chemotherapeutic agents for colorectal cancer. *Oncologist*. 2000;5:99. https://doi.org/10.1634/theoncologist.5-2-99.

57 Baweja R. The theory and practlce of industrial pharmacy. *J Pharm Sci*. 1987;76:90–91. https://doi.org/10.1002/jps.2600760125.

58 Mansoori B, Mohammadi A, Davudian S, Shirjang S, Baradaran B. The different mechanisms of cancer drug resistance: a brief review. *Adv Pharm Bull*. 2017;7:339–348. https://doi.org/10.15171/apb.2017.041.

59 Mahmood A, Lanthaler M, Laffleur F, Huck CW, Bernkop-Schnürch A. Thiolated chitosan micelles: highly mucoadhesive drug carriers. *Carbohydr Polym*. 2017;167:250–258. https://doi.org/10.1016/j.carbpol.2017.03.019.

60 Hua S, Marks E, Schneider JJ, Keely S. Advances in oral nano-delivery systems for colon targeted drug delivery in inflammatory bowel disease: selective targeting to diseased versus healthy tissue. *Nanomed Nanotechnol Biol Med*. 2015;11:1117–1132. https://doi.org/10.1016/j.nano.2015.02.018.

61 Liu F, Ma F, Wang Y, et al. PKM2 methylation by CARM1 activates aerobic glycolysis to promote tumorigenesis. *Nat Cell Biol*. 2017;19:1358–1370. https://doi.org/10.1038/ncb3630.

62 Yue P-F, Lu X-Y, Zhang Z-Z, et al. The study on the entrapment efficiency and in vitro release of puerarin submicron emulsion. *Aaps Pharmscitech*. 2009;10:376–383. https://doi.org/10.1208/s12249-009-9216-3.

63 Mansuri S, Kesharwani P, Tekade RK, Jain NK. Lyophilized mucoadhesive-dendrimer enclosed matrix tablet for extended oral delivery of albendazole. *Eur J Pharm Biopharm*. 2016;102:202–213. https://doi.org/10.1016/j.ejpb.2015.10.015.

64 Fan B, Xing Y, Zheng Y, Sun C, Liang G. pH-responsive thiolated chitosan nanoparticles for oral low-molecular weight heparin delivery: in vitro and in vivo evaluation. *Drug Deliv*. 2016;23:238–247. https://doi.org/10.3109/10717544.2014.909908.

65 Soni N, Soni N, Pandey H, Maheshwari R, Kesharwani P, Tekade RK. Augmented delivery of gemcitabine in lung cancer cells exploring mannose anchored solid lipid nanoparticles. *J Colloid Interface Sci*. 2016;481:107–116. https://doi.org/10.1016/j.jcis.2016.07.020.

66 Muniswamy VJ, Raval N, Gondaliya P, Tambe V, Kalia K, Tekade RK. "Dendrimer-Cationized-Albumin"encrusted polymeric nanoparticle improves BBB penetration and anticancer activity of doxorubicin. *Int J Pharm*. 2019;555:77–99. https://doi.org/10.1016/j.ijpharm.2018.11.035.

67 Sogias IA, Williams AC, Khutoryanskiy VV. Chitosan-based mucoadhesive tablets for oral delivery of ibuprofen. *Int J Pharm*. 2012;436:602–610. https://doi.org/10.1016/j.ijpharm.2012.07.007.

68 Thoorens G, Krier F, Leclercq B, Carlin B, Evrard B. Microcrystalline cellulose, a direct compression binder in a quality by design environment—A review. *Int J Pharm*. 2014;473:64–72. https://doi.org/10.1016/j.ijpharm.2014.06.055.

69 Pingali K, Mendez R, Lewis D, Michniak-Kohn B, Cuitino A, Muzzio F. Mixing order of glidant and lubricant–influence on powder and tablet properties. *Int J Pharm*. 2011;409:269–277. https://doi.org/10.1016/j.ijpharm.2011.02.032.